Geophysical Research Letters

RESEARCH LETTER
10.1029/2019GL083721

Local and Regional Indian Summer Monsoon Precipitation Dynamics During Termination II and the Last Interglacial

Matthias Magiera[1], **Franziska A. Lechleitner**[2], **Andrea M. Erhardt**[3], **Adam Hartland**[4], **Ola Kwiecien**[5], **Hai Cheng**[6,7], **Harold J. Bradbury**[8], **Alexandra V. Turchyn**[8], **Sylvia Riechelmann**[5], **Lawrence Edwards**[7], and **Sebastian F. M. Breitenbach**[5]

[1]Department of Biological and Geographical Sciences, University of Huddersfield, Huddersfield, UK, [2]Department of Earth Sciences, University of Oxford, Oxford, UK, [3]Department of Earth and Environmental Sciences, University of Kentucky, Lexington, KY, USA, [4]Environmental Research Institute, University of Waikato, Hamilton, New Zealand, [5]Institute of Geology, Mineralogy and Geophysics, Ruhr-University Bochum, Bochum, Germany, [6]Institute of Global Environmental Change, Xi'an Jiaotong University, Xi'an, China, [7]Department of Earth Sciences, University of Minnesota, Minneapolis, MN, USA, [8]Department of Earth Sciences, University of Cambridge, Cambridge, UK

Key Points:

- This study represents a first multiproxy stalagmite record from the Indian summer monsoon domain covering Termination II and Marine Isotope Stage 5e
- Combining $\delta^{18}O$, $\delta^{44}Ca$, and elemental data helps to discriminate between rainfall source and amount and local infiltration
- The rainy season during Marine Isotope Stage 5e was wetter, likely with more extreme rainfall events, compared to the Holocene

Supporting Information:

- Supporting Information S1
- Figure S1
- Figure S2
- Figure S3
- Figure S4
- Figure S5
- Figure S6
- Figure S7
- Table S1
- Table S2
- Table S3

Correspondence to:
M. Magiera,
matthias.magiera@gmail.com

Citation:
Magiera, M., Lechleitner, F. A., Erhardt, A. M., Hartland, A., Kwiecien, O., Cheng, H., et al. (2019). Local and regional Indian summer monsoon precipitation dynamics during Termination II and the last interglacial. *Geophysical Research Letters*, *46*, 12,454–12,463. https://doi.org/10.1029/2019GL083721

Received 14 MAY 2019
Accepted 23 SEP 2019
Accepted article online 25 OCT 2019
Published online 14 NOV 2019

Abstract To date Indian summer monsoon (ISM) dynamics have been assessed by changes in stalagmite $\delta^{18}O$. However, stalagmite $\delta^{18}O$ is influenced by multiple environmental factors (e.g., atmospheric moisture transport, rainfall amount at the study site, and ISM seasonality), precluding simple and clear reconstructions of rainfall amount or variability. This study aims to disentangle these environmental factors by combining $\delta^{18}O$, $\delta^{44}Ca$, and elemental data from a stalagmite covering Termination II and the last interglacial from Mawmluh Cave, NE India, to produce a semiquantitative reconstruction of past ISM rainfall. We interpret $\delta^{18}O$ as a mixed signal of rainfall source dynamics and rainfall amount and coupled $\delta^{44}Ca$ and X/Ca ratios as indicators of local infiltration rate and prior calcite precipitation in the karst zone. The wettest conditions in our studied interval (135 and 100 kyrs BP; BP = before present, with the present being 1950 CE) occurred during Marine Isotope Stage 5e. Our multiproxy data set suggests a likely change in seasonal distribution of Marine Isotope Stage 5e rainfall compared to the Holocene; the wet season was longer with higher-than-modern dry season rainfall. Using the last interglacial as an analogue for future anthropogenic warming, our data suggest a more erratic ISM behavior in a warmer world.

1. Introduction

Precipitation in Northeast India is governed by the ISM, which is part of the Asian summer monsoon (ASM) system, one of the largest and most studied atmospheric circulation systems on Earth (Buckley et al., 2014). With the ASM affecting 60% of Earth's population, understanding its present and past dynamics is vital for assessing future risks associated with anthropogenic climate change (e.g., flooding and/or crop failure) (Shukla et al., 2011). While Holocene and modern ISM dynamics are relatively well understood (Berkelhammer et al., 2010; Kathayat et al., 2016; Lechleitner et al., 2017; Myers et al., 2015; Ronay et al., 2019; Sinha et al., 2015; Ziegler et al., 2010), ongoing anthropogenic global warming provides incentive to investigate past periods of even higher global temperatures. One such warm period, the last interglacial (Marine Isotope Stage 5e—MIS-5e (Railsback et al., 2015; Shackleton et al., 2003)), was characterized by minor ice sheet coverage at high latitudes (Berger et al., 2016; Jia et al., 2016; Shackleton et al., 2003; Yin & Berger, 2015), and higher-than-modern temperatures and sea level (Berkelhammer et al., 2010; Burns, 2002; Siccha et al., 2015), and provides a potential analogue for future climate conditions (Fischer et al., 2018).

Here, we present a new multiproxy stalagmite record from Mawmluh Cave, Northeast India, covering the Termination II (T II: 134–130 kyrs BP) to late MIS-5e interval. We combine stalagmite $\delta^{44}Ca$, $\delta^{18}O$, and elemental (X/Ca) measurements with the objective to disentangle local from regional precipitation dynamics. Due to the paucity of well-dated, high-resolution, continental records from the ISM domain covering the penultimate glacial/interglacial transition, we focus in the first instance on process-oriented interpretation of our data rather than comparison with other records.

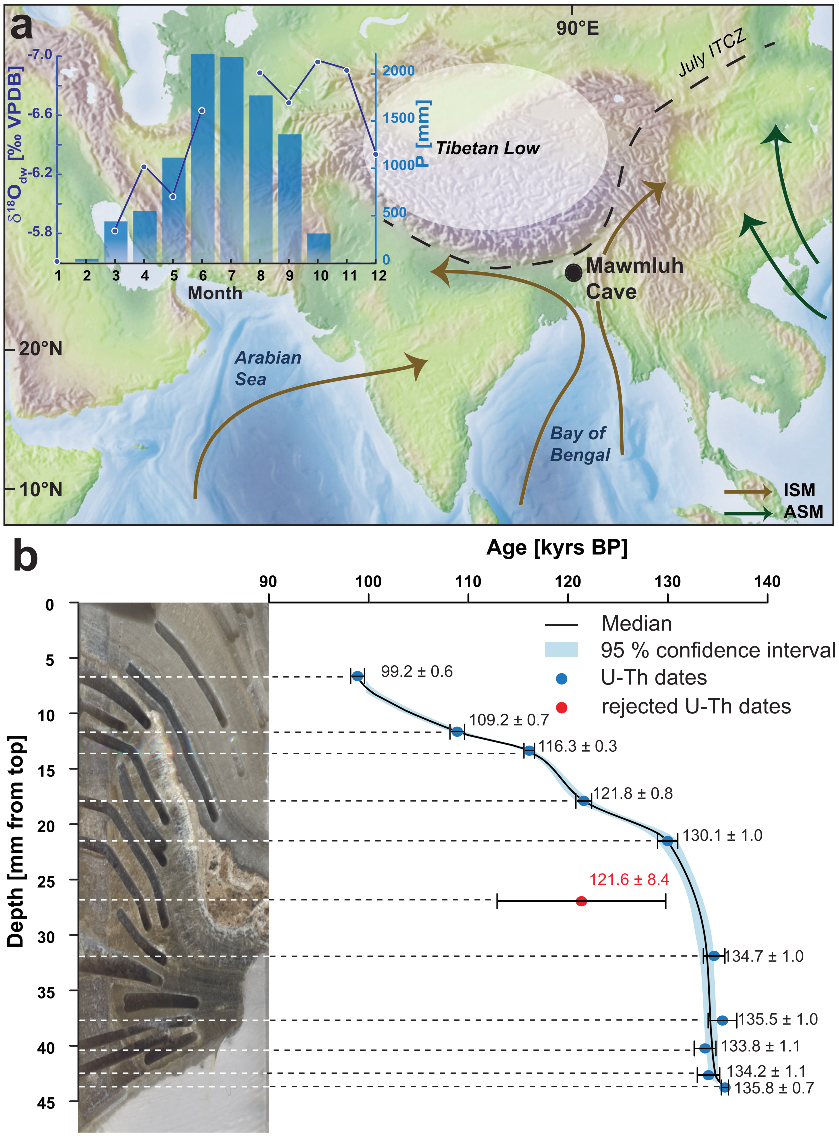

Figure 1. Location of Mawmluh Cave and the summer monsoon branches and sample details: The prevailing wind trajectories of the Indian summer monsoon (ISM) are denoted by brown arrows and by green arrows for the Asian summer monsoon (ASM; adapted from Lechleitner et al., 2017). The climate diagram shows rainfall amount (in mm) and dripwater $\delta^{18}O$ (‰,Vienne Pee-Dee Belemnite [VPDB]) per month (data obtained from Breitenbach et al., 2015); (a) subsample MAW-3_7 and age-depth model based on interpolation between the U-Th dates. Black dots denote U/Th samples with their errors, blue shading indicates the 95% confidence interval and the black line denotes the median of the COnstructing Proxy Records from Age (COPRA) age-depth model (b).

1.1. Study Site and Modern Climate

Mawmluh Cave is located on the Meghalaya Plateau in Northeast India (25°15′44″N, 91°52′54″E, 1160 m above sea level; Figure 1a). Mean annual precipitation at the site amounts to an average of ~10,000 mm per year (http://climexp.knmi.nl), with 75% of rainfall occurring during the ISM season (June to mid-October; Figure 1a). During the ISM season, moisture is delivered to Mawmluh Cave principally by advection of air masses from the Bay of Bengal (BoB) branch of the ISM toward the Meghalaya Plateau. Orographic forcing of the Meghalaya Plateau leads to adiabatic cooling of the air masses and extreme rainfall during the ISM (Figure 1a). Rainfall $\delta^{18}O$ values are lowest during the ISM season, due to a combination of four factors: (i) moisture source location (Asian continent or Indian Ocean), (ii) air mass travel distance from the BoB and the Indian Ocean (rainout effect), (iii) temporal changes in the moisture source isotopic composition due to fresh water runoff from the Asian continent, and (iv) isotopic disequilibrium between seawater and vapor during stormy weather. During the pre-ISM (January to May), higher $\delta^{18}O$ values are indicative of low precipitation, due to a shorter transport pathway as moisture largely originates from the BoB. In the post-ISM months (mid-October to December), a more proximal moisture source in the BoB is combined with a fresh water effect due to increased summer runoff from the Tibetan Plateau, resulting in lower $\delta^{18}O$ values than would be expected from a proximal moisture source (Breitenbach et al., 2010). These changes are also seen in Mawmluh Cave dripwater, where pre-ISM $\delta^{18}O$ is higher than ISM and post-ISM $\delta^{18}O$ (Figure 1a) and $\delta^{18}O$ is highest when infiltration is minimal during the dry season (Breitenbach et al., 2010; Breitenbach et al., 2015). Changes in the timing of the reversal of the circulation patterns (i.e., seasonality) likely have a strong effect on the length and intensity of the wet and dry seasons and thus on ISM "strength," with a longer-lasting ISM resulting in more depleted $\delta^{18}O$.

1.2. Speleothems as Precipitation Archives

To date speleothems are the most robustly dated and highest-resolved archives of ASM precipitation variability (Cai et al., 2015; Cheng et al., 2016; Johnson et al., 2006; Wang et al., 2001; Yuan et al., 2004). Past studies focused on stalagmite $\delta^{18}O$ to explore changes in monsoon intensity, where stalagmite $\delta^{18}O$ is influenced by combined local (e.g., rainfall amount, infiltration patterns within the aquifer, and length of the rainy season) and regional factors (moisture source location and atmospheric transport of water vapor) (Baker et al., 2015; Cheng et al., 2016; Dykoski et al., 2005; Kukla et al., 2019). In general, more negative stalagmite $\delta^{18}O$ is interpreted as higher monsoon intensity, and more positive $\delta^{18}O$ as lower monsoon intensity (Fairchild & Baker, 2012). However, with the multitude of factors influencing speleothem $\delta^{18}O$, reconstructing regional and local monsoon dynamics based on this proxy alone remains challenging (Breitenbach et al., 2010; Dreybrodt & Scholz, 2011; Gupta & Deshpande, 2005; Lechleitner et al., 2017; Pausata et al., 2011).

The key to disentangling local from regional effects in past precipitation patterns lies in the aquifer above the cave. Rainwater leaches Ca from soil and bedrock and transports it to the cave through the karst. Upon reaching the cave, the lower cave atmosphere pCO_2 causes the carbonate and Ca-enriched fluid to degas, resulting in carbonate precipitation. Carbonate precipitation might also occur within the karst zone, e.g., in air-filled pockets, a process termed prior carbonate precipitation (PCP) (Fairchild & Baker, 2012). Infiltration amount is one major factor controlling PCP: Infiltration increases during heavy rainfall, filling pores, and voids within the aquifer with water which in turn increases the velocity of water moving through the karst zone and decreases the residence time of the solution in the aquifer. Together, these processes combine to minimize PCP, while reduced infiltration conversely enhances PCP, thus linking PCP to local rainfall amount (Owen et al., 2016; Sherwin & Baldini, 2011). Apart from infiltration amount, the length of the pathway the water has to cover to reach the cave is a second factor controlling PCP. A longer pathway, with increased water residence time within the karst zone will result in increased PCP. However, when considering variability in PCP over time, the influence of pathway length is likely of secondary importance compared to infiltration amount, and thus using PCP as measure for infiltration amount is justified (Tadros et al., 2016).

Elemental ratios (X/Ca; here Mg/Ca, Sr/Ca, and Ba/Ca) measured in speleothems are the most widely applied proxy for PCP (Fairchild & Baker, 2012). Given the similar size and ionic radii of Mg^{2+}, Sr^{2+}, and Ba^{2+}, the incorporation of these elements into calcite occurs via substitution of Ca^{2+} (Fairchild & Baker, 2012; McIntire, 1963). When PCP occurs in the karst, Ca is incorporated into calcite while incompatible elements stay in solution where their ratio to Ca (X/Ca) increases; this is reflected in increased speleothem X/Ca values.

Since the partitioning of Mg/Ca, Sr/Ca, and Ba/Ca are also influenced by temperature and fluid elemental composition (Day & Henderson, 2013; Fairchild & Baker, 2012), X/Ca values provide important but not yet quantitative information on past karst hydrological changes (Huang & Fairchild, 2001; Owen et al., 2016). Calcium isotope ratios (measured as $\delta^{44/40}Ca$, referred hereafter as $\delta^{44}Ca$) have recently emerged as a promising new proxy for PCP (Owen et al., 2016; Reynard et al., 2011). The $\delta^{44}Ca$ of calcite is influenced by the calcite growth rate, which is controlled by the rate of CO_2 degassing and the saturation state of the solution with respect to calcium carbonate. During carbonate mineral precipitation, light ^{40}Ca isotopes are preferentially incorporated into the precipitate due to kinetic isotope fractionation (Li et al., 2018;

Owen et al., 2016; Reynard et al., 2011; Yan et al., 2016), leaving the fluid enriched in ^{44}Ca. Thus, increased infiltration and minimal PCP during wet periods are expected to result in lower stalagmite δ^{44}Ca values, while periods of reduced infiltration and enhanced PCP will be reflected in increased stalagmite δ^{44}Ca (Owen et al., 2016).

2. Materials and Methods

The 125-cm long stalagmite MAW-3 was collected from Mawmluh Cave in 2007. To evaluate modern seasonal variability in δ^{44}Ca values and calculate a site-specific fractionation factor, we used two modern carbonate precipitates, MAW-Mod-1 (collected from a glass plate in 2007) and MAW-logger (formed on a drip logger in 2013), and compared them to nine dripwater (five pre-ISM, two ISM, and two post-ISM) and two host rock samples, collected in 2007 and 2013 (supporting information in Table S3). The mineralogy of MAW-3_7 and the two modern precipitates was determined using X-ray diffraction on a Panalytical Empyrean powder diffractometer (PANalytical B.V., Almelo, The Netherlands) at Ruhr-University Bochum (RUB). We focus here on the lowermost 7 cm of the sample section MAW-3_7 (Figure 1b). The chronology of MAW-3_7 is constrained by 10 U-Th dates (Figure 1b; Table S2), analyzed by multicollector inductively coupled mass spectrometry using a Thermo Finnigan Neptune in the Minnesota Isotope Laboratory following the methodology of Edwards et al. (1987) and Cheng et al. (2013). The age model was constructed by applying a cubic interpolation procedure using COPRA (Breitenbach et al., 2012).

A total of 108 samples (Table S1 in SI) were milled at a spatial resolution of 0.4 mm along the stalagmite growth axis using a CAM 100 (vhf) micromill at RUB. An aliquot of 87 samples were analyzed for δ^{18}O and δ^{13}C on a ThermoFisher Scientific MAT 235 IRMS equipped with a GasBench II at RUB, following the procedure of Breitenbach and Bernasconi (2011). Based on an in-house carbonate standard, the 1σ reproducibility is ±0.07‰ for δ^{18}O (2015–2016). All values are reported in ‰ relative to the VPDB standard. Aliquots from 25 samples were analyzed for elemental ratios using a Perkin Elmer Elan quadrupole ICP-MS at the University of Waikato; however only 13 out of 25 samples have yielded results due to insufficient sample material. The samples were standardized using a NIST-certified external standard solution (see SI for details). Aliquots of 33 stalagmite samples, the dripwater samples, the modern calcite sample MAW-logger, and two host rock samples were analyzed for δ^{44}Ca ($\delta^{44/40}$Ca) on a ThermoFisher Scientific Triton Plus Thermal Ionisation Mass Spectrometer in the Department of Earth Sciences at the University of Cambridge, following the method of Bradbury and Turchyn (2018). The average external 2σ standard deviation over 9 months on the standard NIST 915B was 0.1‰ (mean = −0.28, n = 82; Text S1 in SI).

The modern aragonite precipitate of MAW-Mod-1 was analyzed for $\delta^{44/42}$Ca on a ThermoFisher Scientific Neptune multicollector inductively coupled mass spectrometry at RUB. The long-term reproducibility of the standard SRM-915a is $\delta^{44/42}\mathrm{Ca}_{\mathrm{IAPSO}} = -0.99 \pm 0.09‰$ (2σ) ($\delta^{44/42}\mathrm{Ca}_{\mathrm{BSE}} = -1.13 \pm 0.19‰$ (2σ); n = 79; January to September 2017), which is in agreement with previously published values (Gussone, Filipsson, et al., 2016; Hippler et al., 2013; Steuber & Buhl, 2006). All calcium isotope data are reported relative to Bulk Silicate Earth (BSE) reference standard.

For a comparison with the Ca isotope values obtained at Cambridge, the $\delta^{44/42}$Ca values measured at RUB are converted to δ^{44}Ca using the following equation (Harouaka et al., 2016):

$$\delta^{44}Ca = \delta^{44/42}Ca * \frac{41.9586}{39.9626} * \frac{39.9626 - 43.9555}{41.9586 - 43.9555} \tag{1}$$

Quantification of PCP was performed following the equations described in Owen et al. (2016) and Gussone, Schmitt, et al. (2016). Equation (2) was used to calculate the present-day site-specific water-calcite fractionation factor using the δ^{44}Ca value of the modern precipitate (denoted as δ_A) and the δ^{44}Ca value of dripwater samples (denoted as δ_B).

$$\alpha = \frac{\delta_A + 1000}{\delta_B + 1000}. \tag{2}$$

Equation (3) is used to calculate the fraction of Ca remaining in solution (*f*) during carbonate precipitation (i.e., calcium depletion), as a measure of PCP (Owen et al., 2016). Variables used here are the δ^{44}Ca value of

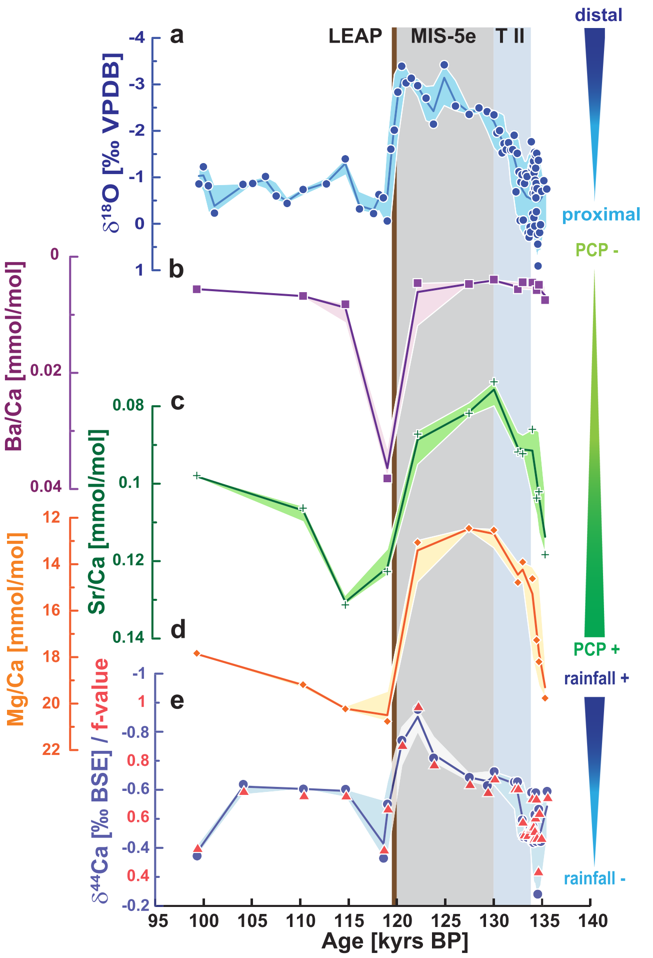

Figure 2. Proxy time series from MAW-3_7: δ^{18}O (a); Ba/Ca (b); Sr/Ca (c); Mg/Ca (d); δ^{44}Ca and f-value (e); blue vertical shading marks T II, the MIS -5e is marked in grey, and the LEAP as brown line. BS = Bulk Silicate Earth; LEAP = Late Eemian Arid Period; MIS = Marine Isotope Stage; PCP = prior carbonate precipitation; VPDB = Vienne Pee-Dee Belemnite.

the calcitic stalagmite (r_s), the initial dripwater δ^{44}Ca value (r_0) before any carbonate precipitation (assumed to be the same as the host rock value), and the δ^{44}Ca fractionation factor ($\alpha^{44/40}$; Eq. (2)) between calcite and an aqueous solution (Gussone, Schmitt, et al., 2016).

$$f = \left(\frac{r_s}{\alpha r_0}\right)^{\frac{1}{\alpha - 1}}. \tag{3}$$

3. Results

3.1. Mineralogy and U-Th Chronology

X-ray diffraction analyses revealed that stalagmite MAW-3_7 and the drip logger sample (MAW-logger) are calcitic, while the second modern carbonate precipitate (MAW-Mod-1) is aragonitic. MAW-3_7 grew from 135 to 99 kyrs BP, covering T II, MIS-5e, and the interval encompassing the Late Eemian Arid Period (LEAP, (Sirocko et al., 2005); Figure 1b). The chronology is well constrained due to high U concentrations, averaging 4 ppm, resulting in 2σ errors between ±729 and ±1432 yr (Table S2 in SI). Relatively low growth rates characterized the penultimate glacial (4 μm/yr) and the LEAP (8 μm/yr), while 10 times higher growth rates were observed during MIS-5e (50 μm/yr). Although 13 samples were drilled from the stalagmite, only 10 were included in the final age model. Two samples were rejected because their ages (~50 kyrs BP) confirmed the presence of a growth hiatus and thus were out of the scope of this study. One sample was excluded because very high Th contents resulted in a large age error (8.4 kyrs).

3.2. Stable Isotopes and Elemental Ratios

MAW-3_7 δ^{18}O ranged from −3.43‰ to 0.91‰ VPDB (Figure 2a). The highest values coincided with T II and the LEAP, and lowest values occurred during MIS-5e. Ba/Ca ratios ranged from 0.004 to 0.038 mmol/mol/Sr/Ca ratios from 0.07 to 0.13 mmol/mol and Mg/Ca ratios from 12 to 21 mmol/mol (Figure 2b–2d). For all elemental ratios, lowest values characterize MIS-5e, while higher values characterize T II and the LEAP. All X/Ca values correlate with each other (Mg/Ca vs. Ba/Ca; $R^2 = 0.27$, $p = 0.07$; Sr/Ca vs. Ba/Ca; $R^2 = 0.28$, $p = 0.07$; Mg/Ca vs. Sr/Ca; $R^2 = 0.87$, $p < 0.0001$; Figure S5 in SI). The Ba/Ca record appears almost constant, except for one value, which is one magnitude higher than the rest of the data and skews the correlation with the other elements (without this data point: Mg/Ca vs. Ba/Ca; $R^2 = 0.73$, $p = 0.0004$; Sr/Ca vs. Ba/Ca; $R^2 = 0.87$, $p < 0.00001$). Despite the improved correlation between elemental ratios when excluding this data point, we refrain from treating it as an outlier, as it coincides with the overall maximum in X/Ca in all records. The δ^{44}Ca values follow the δ^{18}O pattern, ranging from −0.24‰ to −0.88‰ BSE with maxima before and after MIS-5e and lowest δ^{44}Ca during MIS-5e (Figure 2e). We observe a significant positive correlation between δ^{18}O and δ^{44}Ca ($R^2 = 0.89$, $p = 3.0 \times 10^{-7}$) but no significant correlation between Mg/Ca and δ^{44}Ca ($R^2 = 0.5$, $p = 0.15$), Sr/Ca and δ^{44}Ca ($R^2 = 0.34$, $p = 0.26$), and Ba/Ca and δ^{44}Ca ($R^2 = 0.33$, $p = 0.47$; Figure S5).

3.3. Reconstructing PCP Using Ca Isotopes

The modern dripwater δ^{44}Ca values (Table S3 in SI) vary depending on the prevailing season. Pre-ISM season dripwater δ^{44}Ca varies from −0.01‰ to 0.11‰ (mean = 0.05 ± 0.03‰, n = 5), while ISM season samples range from 0.00‰ to 0.05‰ (mean = 0.02 ± 0.03‰, n = 2), and post-ISM waters showed values between 0.02‰ and 0.21‰ (mean = 0.12 ± 0.03‰, n = 2).

MAW-Mod-1 yielded a δ^{44}Ca of −1.31‰ (n = 1) and MAW-logger a δ^{44}Ca of −0.66‰ (n = 1). Coeval measurements of dripwater and glass plate precipitate samples allow for the calculation of the site-specific fractionation factor. We chose the calcitic sample MAW-logger, because MAW-3_7 is also calcitic, and the mean value of all dripwater samples (0.04 ± 0.03‰, n = 9) for our calculations because MAW-logger itself covers several months of precipitation. A site-specific fractionation of $\alpha^{44/40} = 0.99929 \pm 0.00001$ ($\alpha^{44/40} = 0.99865 \pm 0.00001$ for the aragonitic sample MAW-Mod-1) was calculated using equation (1), similar to the effective fractionation factor calculated by Owen et al. (2016) for Heshang Cave ($\alpha = 0.99937 \pm 0.00003$). Stalagmite δ^{44}Ca ranged from −0.88‰ to 0.24‰ (Figure 2e). Using the stalagmite δ^{44}Ca, the site-specific fractionation factor α, and the host rock δ^{44}Ca value (mean: −0.15‰ BSE, n = 2; Table S3 in SI), which we use to estimate the initial δ^{44}Ca of the dripwater prior to any calcite precipitation, in equation (2) yielded Ca-depletion values (*f*-values) between 1.00 and 0.42 (i.e., between 0% and 58% Ca-depletion, Figure 2e).

4. Discussion

The interpretation of speleothem δ^{18}O requires detailed understanding of atmospheric circulation and local climate conditions, such as temperature and precipitation seasonality, rainfall transport pathway, effective infiltration, and vegetation cover (Baker et al., 2015; Breitenbach et al., 2010, 2015; Lachniet, 2009; McDermott, 2004). This multitude of influencing factors severely hampers quantitative reconstruction of absolute rainfall changes. Using δ^{18}O, X/Ca, and δ^{44}Ca in tandem with modern monitoring data allows us to disentangle local and regional precipitation dynamics using a semiquantitative approach.

4.1. Oxygen Isotopes as Tracers of Moisture Source

At Mawmluh Cave, variations in precipitation δ^{18}O reflect a mixed signal of moisture source and rainfall amount (Baker et al., 2015; Breitenbach et al., 2010, 2015). During the premonsoon and post-monsoon seasons, the dominant air mass trajectories stem from the proximal BoB, delivering rainwater with relatively high δ^{18}O values. With the onset of the ISM, the moisture source shifts to the open Indian Ocean and the Arabian Sea, and the longer transport path lowers the δ^{18}O of ISM rainfall. Based on our current understanding, local rainfall δ^{18}O generally reflects moisture source variability across the Indian Ocean and, in broad terms, regional moisture dynamics (Baker et al., 2015).

The *length* of the monsoon season also likely impacts speleothem δ^{18}O. During the ISM, surface air relative humidity approaches 100%, minimizing reevaporation of raindrops during their fall through the below-cloud atmosphere. Hence, dripwater reaching the cave would have δ^{18}O values close to original unaltered rainfall, yielding more negative speleothem δ^{18}O values during periods with, on average, longer wet seasons. This has been previously recognized in speleothem δ^{18}O records from northern India and China (Cheng et al., 2009; Kathayat et al., 2016; Orland et al., 2015). Although mixing of infiltration waters above Mawmluh Cave results in some buffering, a very short (<1 month) isotope signal transfer time (lag) from rain to drip means that such changes in wet season length should be detectable in speleothems at this location (Breitenbach et al., 2015). However, because of the multiple processes affecting δ^{18}O, this proxy alone cannot be used to disentangle whether the amount of ISM rainfall or its seasonal distribution changed. Instead, a combination of δ^{18}O and PCP proxies should allow us to detect changes in seasonality (Ronay et al., 2019). With ISM rainfall in the range of thousands of mm per ISM season, only an extreme reduction in precipitation amount would induce PCP during the ISM. It is more likely that our PCP proxies (X/Ca and δ^{44}Ca) indicate changes in the dryness and length of the dry season.

4.2. Trace Element Ratios as PCP Recorders

X/Ca ratios are useful tracers of changes in seasonal water availability. In Mawmluh Cave, trace element incorporation in speleothems is governed by PCP, which is recognized to occur mainly during the dry and pre-ISM seasons (Ronay et al., 2019). PCP is minimized during the ISM (and post-ISM) when the cave floods and the karst zone is waterlogged. Thus, it is dry and pre-ISM season infiltration which acts as the governing parameter for PCP, informing us on dry season length and reversely ISM duration.

X/Ca ratios are therefore valuable tracers of past *dry season dryness*. Under locally drier conditions, PCP-sensitive Mg/Ca, Sr/Ca, and Ba/Ca ratios in MAW-3_7 increase, while they decrease under wetter conditions (Figure 2). X/Ca increases can be induced by either a shortened ISM (and thus increased rainfall seasonality) or a reduction in dry season rainfall amount (increased dry season dryness) or a combination of both.

Additionally, ventilation-related changes in cave air pCO_2 can influence PCP occurring in the cave and/or epikarst. Stronger ventilation (lower pCO_2) leads to increased PCP, and weaker ventilation (higher pCO_2) to decreased PCP (Ronay et al., 2019). While the direction of seasonal ventilation changes is corroborated by dry/monsoon season changes, separating the signal of PCP induced by infiltration or by changes in cave air pCO_2 remains challenging. However, Mawmluh Cave experiences only minor seasonal variations in pCO_2 levels, and thus the effect of pCO_2 on PCP is likely minimal, especially when compared to much larger amplitude changes in infiltration. Consequently, we propose rainfall amount as the major controlling factor on PCP.

4.3. Calcium Depletion as Infiltration and PCP Recorder

Under the assumption of linear scaling of PCP versus rainfall change, a quantitative PCP reconstruction would also allow the quantification of past rainfall amount. Ideally, Ca isotopes should be calibrated against local moisture balance, but in our case, this goal could not be met due to logistical challenges, as the cave floods to the ceiling in the wet season. Hence, our interpretation of δ^{44}Ca remains semiquantitative.

Although we cannot reconstruct rainfall *amount* quantitatively, we can use δ^{44}Ca values for a semiquantitative reconstruction of PCP dynamics. For this, we use the Ca-depletion values (f-values; Eq. (3)), where low δ^{44}Ca yields high f-values and vice versa (Figure 2e). During PCP, lighter isotopes leave the percolating water preferentially, leading to higher δ^{44}Ca values in the remaining solution. In times of high infiltration, PCP will be diminished due to high water pressure heads and low residence times, resulting in lower δ^{44}Ca and higher f-values. During times of low infiltration, that is, dry seasons, PCP is enhanced and recorded as high δ^{44}Ca and low f-values. This relationship is mirrored in modern dripwater, where δ^{44}Ca values are lower during the ISM than during the dry season (Figure S6).

4.4. ISM Dynamics During T II, MIS-5e, and the LEAP

Combining the isotopic and elemental data, we can characterize ISM dynamics between 135 and 99 kyrs BP and semiquantitatively estimate PCP changes (Figure 2). This allows us to disentangle local conditions at the cave site from regional circulation dynamics.

T II was characterized by higher δ^{18}O, δ^{44}Ca, and X/Ca values, reflecting a more proximal moisture source, enhanced dry season PCP, and possibly a longer dry season. Increased PCP due to an enhanced/prolonged dry season is also reflected in the very low f-values ($f = 0.42$ to 0.68), which translate to a reduction in dry season precipitation of 10% to 44% relative to modern conditions (Figure S7), if linear correlation between δ^{18}O and δ^{44}Ca is assumed (Owen et al., 2016). As discussed above, this assumption remains untested, and the calculated precipitation amounts will need to be carefully evaluated in future studies. Our results are in line with earlier findings of a weaker ISM during T II (Cheng et al., 2009; Kathayat et al., 2016).

During MIS-5e (132–116 kyrs BP), lower δ^{18}O values relative to T II suggest a strong ISM with a distal moisture source and possibly increased summer rainfall and an overall longer wet season. Lower δ^{44}Ca and X/Ca ratios suggest minimal PCP during the dry season, likely suppressed by increased dry season (post-ISM and pre-ISM) rainfall (Figure 3). From T II until the end of MIS-5e, f-values rise continuously, ranging from 0.70 to 1.0, suggesting an overall increase in dry season precipitation between T II and MIS-5e of up to 60% and an increase of up to 25% relative to modern conditions (Figure 2; S7).

With the onset of the LEAP, δ^{18}O, δ^{44}Ca, and X/Ca ratios increase, suggesting a weakening ISM, with weakened circulation and decreased rainfall amount (δ^{18}O), a prolonged dry season, and enhanced PCP (δ^{44}Ca and X/Ca). Up to 50% reductions in dry season precipitation relative to MIS-5e are observed.

In comparison with Holocene stalagmite δ^{18}O values from Mawmluh Cave (Berkelhammer et al., 2012; Dutt et al., 2015; Lechleitner et al., 2017), the values in MAW-3_7 during MIS-5e are ~4‰ higher. Moreover, δ^{44}Ca values during MIS-5e are lower than in the modern precipitates (i.e., our reference point).

This seems counterintuitive, as the warmer MIS-5e should result in a stronger ISM (Fischer et al., 2018) with lower δ^{18}O values than during the Holocene. At the same time, lower δ^{44}Ca values support the idea of a stronger ISM during MIS-5e with a wetter dry season leading to a reduction in PCP. Unless these

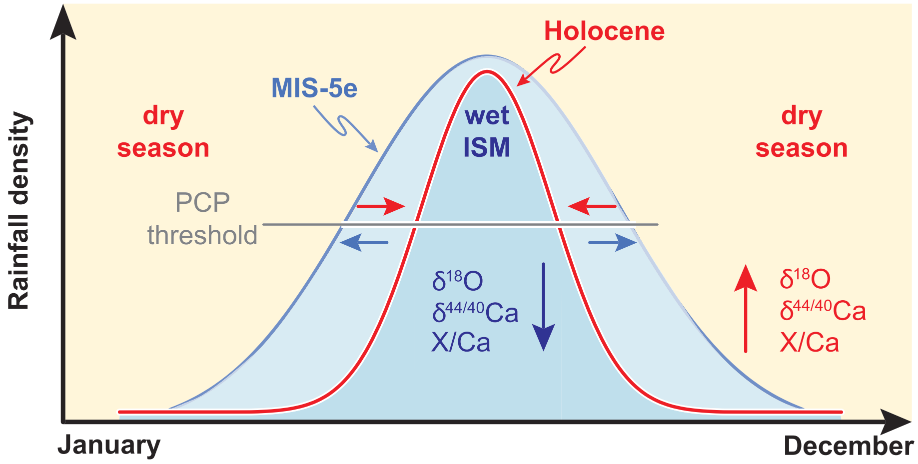

Figure 3. Conceptual model of the meteorological year with rainfall events increasing during the Indian summer monsoon (ISM) and decreasing during the dry season. Hypothesized rainfall distributions are denoted red for the Holocene and blue for MIS-5e. The grey line denotes the prior carbonate precipitation (PCP) threshold below which PCP is expected and thus the transition from dry season to monsoon season. We assume that MIS-5e was characterized by increased dry season rainfall and increased summer rainfall with abundant extreme events compared to the Holocene. During the dry season, rainfall $\delta^{18}O$ and PCP increase (higher $\delta^{44}Ca$ and X/Ca). During the ISM, the amount effect is almost negligible, while Rayleigh fractionation leads to lower $\delta^{18}O$ values and increased infiltration minimized PCP ($\delta^{44}Ca$ and X/Ca decrease). MIS = Marine Isotope Stage.

offsets are caused by changes in flow paths and mixing history, it is likely MIS-5e was characterized by a change in seasonality with increased dry season infiltration and decreased PCP compared to present times (Figure 3).

Increased dry season rainfall would be prone to enhanced reevaporation of early (pre-ISM) and late (post-ISM) rainfall at the cave site, resulting in higher rainfall $\delta^{18}O$ throughout MIS-5e. At the same time, increased dry season rainfall would minimize PCP and lead to decreased X/Ca and $\delta^{44}Ca$ values relative to the Holocene. Thus, our record suggests very strong PCP during T II and the LEAP, reduced PCP during MIS-5e, and some PCP occurring during the Holocene. Additional X/Ca and $\delta^{44}Ca$ data covering the Holocene are needed to test this hypothesis.

If our proposed scenario is correct, a warmer atmosphere in the near future would lead to an intensified ISM season and a wetter dry season (possibly with more extreme events like droughts and floods (Malik et al., 2016)).

5. Conclusions

A high-resolution stalagmite multiproxy ISM record documents, for the first time, regional and local dynamics of T II and last interglacial rainfall in Northeast India. The combination of $\delta^{18}O$, $\delta^{44}Ca$, and X/Ca ratios unequivocally suggests that during T II and the LEAP, conditions were drier than during MIS-5e. Furthermore, in comparison to the Holocene, MIS-5e was likely characterized by a different seasonal distribution of precipitation. We propose that overall the ISM season and the dry season were characterized by higher-than-modern rainfall. This scenario would explain the apparent incongruency between higher-than-modern stalagmite $\delta^{18}O$ (regional signal) and the simultaneously reduced PCP in the karst zone (local signal) during MIS-5e.

Coupling $\delta^{44}Ca$ with X/Ca ratios provides a well-reasoned, semiquantitative approximation of past rainfall amount. While the accuracy of our tentative reconstruction remains to be validated in future research, it enables the local precipitation signal to be extracted from the regional pattern and represents a significant step toward quantification of past rainfall changes, especially in regions with strong rainfall seasonality.

Acknowledgments

This study received funding from the European Union's Horizon 2020 research and innovation programme under the Marie Skłodowska-Curie grant 691037 (to SFMB, OK, AH). Calcium isotope analyses were supported through ERC StG 307582 CARBONSINK (to AVT) and NERC NE/R013519/1 (to HJB). Financial support came from the National Natural Science Foundation of China (NSFC-41731174, to HC and LE), an award from the palaeoclimate program by the National Science Foundation (NSF-1702816, to HC and LE), and a Rutherford Discovery Fellowship award (RDF-UOW1601, to AH). Gregory Diengdoh (Shillong) is thanked for helping during sampling and Ingrid Lindeman (University of Waikato) for assistance in measuring trace elements. We thank Beate Gehnen for assisting with stable isotope analysis. We thank Daniel E. Ibarra and an anonymous reviewer for their critical feedback on earlier versions of this manuscript and the editorial team of GRL for handling our submission All data will be archived on the NOAA website (https://www.ncdc.noaa.gov/paleo/study/27990).

References

Baker, A. J., Sodemann, H., Baldini, J. U. L., Breitenbach, S. F. M., Johnson, K. R., van Hunen, J., & Zhang, P. (2015). Seasonality of westerly moisture transport in the East Asian summer monsoon and its implications for interpreting precipitation δ 18 O. *Journal of Geophysical Research: Atmospheres*, *120*, 5850–5862. https://doi.org/10.1002/2014JD022919

Berger, A., Crucifix, M., Hodell, D. A., Mangili, C., McManus, J. F., Otto-Bliesner, B., et al. (2016). Interglacials of the last 800,000 years. *Reviews of Geophysics*, *54*, 162–219. https://doi.org/10.1002/2015RG000482

Berkelhammer, M., Sinha, A., Mudelsee, M., Cheng, H., Edwards, R. L., & Cannariato, K. (2010). Persistent multidecadal power of the Indian summer monsoon. *Earth and Planetary Science Letters*, *290*(1-2), 166–172. https://doi.org/10.1016/j.epsl.2009.12.017

Berkelhammer, M., Sinha, A., Stott, L., Cheng, H., Pausata, F. S. R., & Yoshimura, K. (2012). An Abrupt Shift in the Indian Monsoon 4000 Years Ago. In L. Giosan (Ed.), *Climates, landscapes, and civilizations*, *Geophysical Monograph Series* (Vol. 198, pp. 75–88). Washington, DC: American Geophysical Union.

Bradbury, H. J., & Turchyn, A. V. (2018). Calcium isotope fractionation in sedimentary pore fluids from ODP Leg 175: Resolving carbonate recrystallization. *Geochimica et Cosmochimica Acta*, *236*, 121–139. https://doi.org/10.1016/j.gca.2018.01.040

Breitenbach, S. F. M., Adkins, J. F., Meyer, H., Marwan, N., Kumar, K. K., & Haug, G. H. (2010). Strong influence of water vapor source dynamics on stable isotopes in precipitation observed in Southern Meghalaya, NE India. *Earth and Planetary Science Letters*, *292*(1-2), 212–220. https://doi.org/10.1016/j.epsl.2010.01.038

Breitenbach, S. F. M., & Bernasconi, S. M. (2011). Carbon and oxygen isotope analysis of small carbonate samples (20 to 100 μg) with a GasBench II preparation device. *Rapid Communications in Mass Epectrometry: RCM*, *25*(13), 1910–1914. https://doi.org/10.1002/rcm.5052

Breitenbach, S. F. M., Lechleitner, F. A., Meyer, H., Diengdoh, G., Mattey, D., & Marwan, N. (2015). Cave ventilation and rainfall signals in dripwater in a monsoonal setting—A monitoring study from NE India. *Chemical Geology*, *402*, 111–124. https://doi.org/10.1016/j.chemgeo.2015.03.011

Breitenbach, S. F. M., Rehfeld, K., Goswami, B., Baldini, J. U. L., Ridley, H. E., Kennett, D. J., et al. (2012). Constructing Proxy Records from Age models (COPRA). *Climate of the Past*, *8*(5), 1765–1779. https://doi.org/10.5194/cp-8-1765-2012

Buckley, B. M., Fletcher, R., Wang, S.-Y. S., Zottoli, B., & Pottier, C. (2014). Monsoon extremes and society over the past millennium on mainland Southeast Asia. *Quaternary Science Reviews*, *95*, 1–19. https://doi.org/10.1016/j.quascirev.2014.04.022

Burns, S. J. (2002). A 780-year annually resolved record of Indian Ocean monsoon precipitation from a speleothem from south Oman. *Journal of Geophysical Research*, *107*(D20), 518. https://doi.org/10.1029/2001JD001281

Cai, Y., Fung, I. Y., Edwards, R. L., An, Z., Cheng, H., Lee, J.-E., et al. (2015). Variability of stalagmite-inferred Indian monsoon precipitation over the past 252,000 y. *Proceedings of the National Academy of Sciences of the United States of America*, *112*(10), 2954–2959. https://doi.org/10.1073/pnas.1424035112

Cheng, H., Edwards, R. L., Broecker, W. S., Denton, G. H., Kong, X., Wang, Y., et al. (2009). Ice age terminations. *Science (New York, N.Y.)*, *326*(5950), 248–252. https://doi.org/10.1126/science.1177840

Cheng, H., Edwards, R. L., Sinha, A., Spötl, C., Yi, L., Chen, S., et al. (2016). The Asian monsoon over the past 640,000 years and ice age terminations. *Nature*, *534*(7609), 640–646. https://doi.org/10.1038/nature18591

Cheng, H., Lawrence Edwards, R., Shen, C.-C., Polyak, V. J., Asmerom, Y., Woodhead, J., et al. (2013). Improvements in 230Th dating, 230Th and 234 U half-life values, and U–Th isotopic measurements by multi-collector inductively coupled plasma mass spectrometry. *Earth and Planetary Science Letters*, *371-372*, 82–91. https://doi.org/10.1016/j.epsl.2013.04.006

Day, C. C., & Henderson, G. M. (2013). Controls on trace-element partitioning in cave-analogue calcite. *Geochimica et Cosmochimica Acta*, *120*, 612–627. https://doi.org/10.1016/j.gca.2013.05.044

Dreybrodt, W., & Scholz, D. (2011). Climatic dependence of stable carbon and oxygen isotope signals recorded in speleothems: From soil water to speleothem calcite. *Geochimica et Cosmochimica Acta*, *75*(3), 734–752. https://doi.org/10.1016/j.gca.2010.11.002

Dutt, S., Gupta, A. K., Clemens, S. C., Cheng, H., Singh, R. K., Kathayat, G., & Edwards, R. L. (2015). Abrupt changes in Indian summer monsoon strength during 33,800 to 5500 years B. P. *Geophysical Research Letters*, *42*, 5526–5532. https://doi.org/10.1002/2015GL064015

Dykoski, C. A., Edwards, R. L., Cheng, H., Yuan, D., Cai, Y., Zhang, M., et al. (2005). A high-resolution, absolute-dated Holocene and deglacial Asian monsoon record from Dongge Cave, China. *Earth and Planetary Science Letters*, *233*(1-2), 71–86. https://doi.org/10.1016/j.epsl.2005.01.036

Edwards, R. L., Chen, J. H., & Wasserburg, G. J. (1987). 238U234U230Th232Th systematics and the precise measurement of time over the past 500,000 years. *Earth and Planetary Science Letters*, *81*(2-3), 175–192. https://doi.org/10.1016/0012-821X(87)90154-3

Fairchild, I. J., & Baker, A. (2012). *Speleothem Science*. Chichester, UK: John Wiley & Sons, Ltd.

Fischer, H., Meissner, K. J., Mix, A. C., Abram, N. J., Austermann, J., Brovkin, V., et al. (2018). Palaeoclimate constraints on the impact of 2 °C anthropogenic warming and beyond. *Nature Geoscience*, *11*(7), 474–485. https://doi.org/10.1038/s41561-018-0146-0

Gupta, S., & Deshpande, R. (2005). The need and potential applications of a network for monitoring of isotopes in waters of India. *Current Science*, *88*(1), 107–118. Retrieved from www.jstor.org/stable/24110100

Gussone, N., Filipsson, H. L., & Kuhnert, H. (2016). Mg/Ca, Sr/Ca and Ca isotope ratios in benthonic foraminifers related to test structure, mineralogy and environmental controls. *Geochimica et Cosmochimica Acta*, *173*, 142–159. https://doi.org/10.1016/j.gca.2015.10.018

Gussone, N., Schmitt, A.-D., Heuser, A., Wombacher, F., Dietzel, M., Tipper, E., & Schiller, M. (2016). *Calcium Stable Isotope Geochemistry*, *Advances in Isotope Geochemistry* (p. 269). Berlin, Heidelberg: Springer Berlin Heidelberg.

Harouaka, K., Mansor, M., Macalady, J. L., & Fantle, M. S. (2016). Calcium isotopic fractionation in microbially mediated gypsum precipitates. *Geochimica et Cosmochimica Acta*, *184*, 114–131. https://doi.org/10.1016/j.gca.2016.03.003

Hippler, D., Witbaard, R., van Aken, H. M., Buhl, D., & Immenhauser, A. (2013). Exploring the calcium isotope signature of Arctica islandica as an environmental proxy using laboratory- and field-cultured specimens. *Palaeogeography, Palaeoclimatology, Palaeoecology*, *373*, 75–87. https://doi.org/10.1016/j.palaeo.2011.11.015

Huang, Y., & Fairchild, I. J. (2001). Partitioning of Sr2+ and Mg2+ into calcite under karst-analogue experimental conditions. *Geochimica et Cosmochimica Acta*, *65*(1), 47–62. https://doi.org/10.1016/s0016-7037(00)00513-5

Jia, J., Xia, D., Wang, Y., Wang, B., Lu, H., & Zhao, S. (2016). East Asian monsoon evolution during the Eemian, as recorded in the western Chinese Loess Plateau. *Quaternary International*, *399*, 156–164. https://doi.org/10.1016/j.quaint.2015.04.006

Johnson, K. R., Lynn Ingram, B., Sharp, W. D., & Zhang, P. (2006). East Asian summer monsoon variability during Marine Isotope Stage 5 based on speleothem δ18O records from Wanxiang Cave, central China. *Palaeogeography, Palaeoclimatology, Palaeoecology*, *236*(1-2), 5–19. https://doi.org/10.1016/j.palaeo.2005.11.041

Kathayat, G., Cheng, H., Sinha, A., Spötl, C., Edwards, R. L., Zhang, H., et al. (2016). Indian monsoon variability on millennial-orbital timescales. *Scientific Reports*, *6*(1), 24374. https://doi.org/10.1038/srep24374

Kukla, T., Winnick, M. J., Maher, K., Ibarra, D. E., & Chamberlain, C. P. (2019). The sensitivity of terrestrial δ^{18}O gradients to hydroclimate evolution. *Journal of Geophysical Research: Atmospheres*, *124*(2), 563–582. https://doi.org/10.1029/2018JD029571

Lachniet, M. S. (2009). Climatic and environmental controls on speleothem oxygen-isotope values. *Quaternary Science Reviews*, *28*(5-6), 412–432. https://doi.org/10.1016/j.quascirev.2008.10.021

Lechleitner, F. A., Breitenbach, S. F. M., Rehfeld, K., Ridley, H. E., Asmerom, Y., Prufer, K. M., et al. (2017). Tropical rainfall over the last two millennia: Evidence for a low-latitude hydrologic seesaw. *Scientific Reports*, *7*(1), 45809. https://doi.org/10.1038/srep45809

Li, X., Cui, X., He, D., Liao, J., & Hu, C. (2018). Evaluation of the Heshang Cave stalagmite calcium isotope composition as a paleohydrologic proxy by comparison with the instrumental precipitation record. *Scientific Reports*, *8*(1), 2615. https://doi.org/10.1038/s41598-018-20776-5

Malik, N., Bookhagen, B., & Mucha, P. J. (2016). Spatiotemporal patterns and trends of Indian monsoonal rainfall extremes. *Geophysical Research Letters*, *43*, 1710–1717. https://doi.org/10.1002/2016GL067841

McDermott, F. (2004). Palaeoclimate reconstruction from stable isotope variations in speleothems: A review. *Quaternary Science Reviews*, *23*(7-8), 901–918. https://doi.org/10.1016/j.quascirev.2003.06.021

McIntire, W. L. (1963). Trace element partition coefficients—A review of theory and applications to geology. *Geochimica et Cosmochimica Acta*, *27*(12), 1209–1264. https://doi.org/10.1016/0016-7037(63)90049-8

Myers, C. G., Oster, J. L., Sharp, W. D., Bennartz, R., Kelley, N. P., Covey, A. K., & Breitenbach, S. F. M. (2015). Northeast Indian stalagmite records Pacific decadal climate change: Implications for moisture transport and drought in India. *Geophysical Research Letters*, *42*, 4124–4132. https://doi.org/10.1002/2015GL063826

Orland, I. J., Edwards, R. L., Cheng, H., Kozdon, R., Cross, M., & Valley, J. W. (2015). Direct measurements of deglacial monsoon strength in a Chinese stalagmite. *Geology*, *43*(6), 555–558. https://doi.org/10.1130/G36612.1

Owen, R. A., Day, C. C., Hu, C.-Y., Liu, Y.-H., Pointing, M. D., Blättler, C. L., & Henderson, G. M. (2016). Calcium isotopes in caves as a proxy for aridity: Modern calibration and application to the 8.2 kyr event. *Earth and Planetary Science Letters*, *443*(443), 129–138. https://doi.org/10.1016/j.epsl.2016.03.027

Pausata, F. S. R., Battisti, D. S., Nisancioglu, K. H., & Bitz, C. M. (2011). Chinese stalagmite δ18O controlled by changes in the Indian monsoon during a simulated Heinrich event. *Nature Geoscience*, *4*(7), 474–480. https://doi.org/10.1038/ngeo1169

Railsback, L. B., Gibbard, P. L., Head, M. J., Voarintsoa, N. R. G., & Toucanne, S. (2015). An optimized scheme of lettered marine isotope substages for the last 1.0 million years, and the climatostratigraphic nature of isotope stages and substages. *Quaternary Science Reviews*, *111*, 94–106. https://doi.org/10.1016/j.quascirev.2015.01.012

Reynard, L. M., Day, C. C., & Henderson, G. M. (2011). Large fractionation of calcium isotopes during cave-analogue calcium carbonate growth. *Geochimica et Cosmochimica Acta*, *75*(13), 3726–3740. https://doi.org/10.1016/j.gca.2011.04.010

Ronay, E. R., Breitenbach, S. F. M., & Oster, J. L. (2019). Sensitivity of speleothem records in the Indian summer monsoon region to dry season infiltration. *Scientific Reports*, *9*(1), 1–10. https://doi.org/10.1038/s41598-019-41630-2

Shackleton, N. J., Sánchez-Goñi, M. F., Pailler, D., & Lancelot, Y. (2003). Marine Isotope Substage 5e and the Eemian Interglacial. *Global and Planetary Change*, *36*(3), 151–155. https://doi.org/10.1016/S0921-8181(02)00181-9

Sherwin, C. M., & Baldini, J. U. L. (2011). Cave air and hydrological controls on prior calcite precipitation and stalagmite growth rates: Implications for palaeoclimate reconstructions using speleothems. *Geochimica et Cosmochimica Acta*, *75*(14), 3915–3929. https://doi.org/10.1016/j.gca.2011.04.020

Shukla, R. P., Tripathi, K. C., Pandey, A. C., & Das, I. M. L. (2011). Prediction of Indian summer monsoon rainfall using Niño indices: A neural network approach. *Atmospheric Research*, *102*(1-2), 99–109. https://doi.org/10.1016/j.atmosres.2011.06.013

Siccha, M., Biton, E., & Gildor, H. (2015). Red Sea circulation during marine isotope stage 5e. *Paleoceanography*, *30*, 384–401. https://doi.org/10.1002/2013PA002603

Sinha, A., Kathayat, G., Cheng, H., Breitenbach, S. F. M., Berkelhammer, M., Mudelsee, M., et al. (2015). Trends and oscillations in the Indian summer monsoon rainfall over the last two millennia. *Nature Communications*, *6*(1), 6309. https://doi.org/10.1038/ncomms7309

Sirocko, F., Seelos, K., Schaber, K., Rein, B., Dreher, F., Diehl, M., et al. (2005). A late Eemian aridity pulse in Central Europe during the last glacial inception. *Nature*, *436*(7052), 833–836. https://doi.org/10.1038/nature03905

Steuber, T., & Buhl, D. (2006). Calcium-isotope fractionation in selected modern and ancient marine carbonates. *Geochimica et Cosmochimica Acta*, *70*(22), 5507–5521. https://doi.org/10.1016/j.gca.2006.08.028

Tadros, C. V., Treble, P. C., Baker, A., Fairchild, I., Hankin, S., Roach, R., et al. (2016). ENSO–cave drip water hydrochemical relationship: A 7-year dataset from South-Eastern Australia. *Hydrology and Earth System Sciences*, *20*(11), 4625–4640. https://doi.org/10.5194/hess-20-4625-2016

Wang, Y. J., Cheng, H., Edwards, R. L., An, Z. S., Wu, J. Y., Shen, C. C., & Dorale, J. A. (2001). A high-resolution absolute-dated late Pleistocene Monsoon record from Hulu Cave, China. *Science (New York, N.Y.)*, *294*(5550), 2345–2348. https://doi.org/10.1126/science.1064618

Yan, H., Schmitt, A.-D., Liu, Z., Gangloff, S., Sun, H., Chen, J., & Chabaux, F. (2016). Calcium isotopic fractionation during travertine deposition under different hydrodynamic conditions: Examples from Baishuitai (Yunnan, SW China). *Chemical Geology*, *426*, 60–70. https://doi.org/10.1016/j.chemgeo.2016.02.002

Yin, Q., & Berger, A. (2015). Interglacial analogues of the Holocene and its natural near future. *Quaternary Science Reviews*, *120*, 28–46. https://doi.org/10.1016/j.quascirev.2015.04.008

Yuan, D., Cheng, H., Edwards, R. L., Dykoski, C. A., Kelly, M. J., Zhang, M., et al. (2004). Timing, duration, and transitions of the last interglacial Asian monsoon. *Science (New York, N.Y.)*, *304*(5670), 575–578. https://doi.org/10.1126/science.1091220

Ziegler, M., Lourens, L. J., Tuenter, E., Hilgen, F., Reichart, G.-J., & Weber, N. (2010). Precession phasing offset between Indian summer monsoon and Arabian Sea productivity linked to changes in Atlantic overturning circulation. *Paleoceanography*, *25*, PA3213. https://doi.org/10.1029/2009PA001884